Editors' Suggestion

Paramagnetic Singularities of the Orbital Magnetism in Graphene with a Moiré Potential

J. Vallejo Bustamante,[1] R. Ribeiro-Palau,[2] C. Fermon,[3] M. Pannetier-Lecoeur,[3] K. Watanabe,[4] T. Tanigushi,[5] R. Deblock,[1] S. Guéron,[1] M. Ferrier,[1] J. N. Fuchs,[6] G. Montambaux,[1] F. Piéchon,[1] and H. Bouchiat[1]

[1]*Université Paris-Saclay, CNRS, Laboratoire de Physique des Solides, 91405 Orsay, France*
[2]*Université Paris-Saclay, CNRS, C2N, 91120 Palaiseau, France*
[3]*SPEC, CEA, CNRS, Université Paris-Saclay, 91191 Gif-sur-Yvette, France*
[4]*Research Center for Functional Materials, National Institute for Materials Science, 1-1 Namiki, Tsukuba 305-0044, Japan*
[5]*International Center for Materials Nanoarchitectonics, National Institute for Materials Science, 1-1 Namiki, Tsukuba 305-0044, Japan*
[6]*Sorbonne Université, CNRS, Laboratoire de Physique Théorique de la Matière Condensée, LPTMC, 75005 Paris, France*

(Received 13 March 2023; accepted 7 July 2023; published 11 September 2023)

The recent detection of the singular diamagnetism of Dirac electrons in a single graphene layer paved a new way of probing 2D quantum materials through the measurement of equilibrium orbital currents which cannot be accessed in usual transport experiments. Among the theoretical predictions is an intriguing orbital paramagnetism at saddle points of the dispersion relation. Here we present magnetization measurements in graphene monolayers aligned on hexagonal boron nitride crystals. Besides the sharp diamagnetic McClure response at the Dirac point, we detect extra diamagnetic singularities at the satellite Dirac points of the moiré lattice. Surrounding these diamagnetic satellite peaks, we also observe paramagnetic peaks located at the chemical potential of the saddle points of the graphene moiré band structure and relate them to the presence of van Hove logarithmic singularities in the density of states. These findings reveal the long ago predicted anomalous paramagnetic orbital response in 2D systems when the Fermi energy is tuned to the vicinity of saddle points.

DOI: 10.1103/PhysRevLett.131.116201

Landau diamagnetism originates from the quantum orbital motion of delocalized electrons at low magnetic field. In systems with a periodic potential, this orbital magnetism depends on the specific properties of the lattice. The orbital susceptibility of a single band system is proportional to the curvature of the energy dispersion relation (i.e., the inverse effective mass of carriers). This is known as the Landau-Peierls result [1,2]. In multiband systems, the coupling induced by the magnetic field between Bloch wave functions of different bands gives rise to new effects. The zero-field susceptibility is then not only determined by the curvature of the bands, but also by geometrical properties of Bloch functions such as the Berry curvature in reciprocal space [3–5]. For instance, a divergent diamagnetism of graphene at the Dirac point (DP) was predicted by McClure [6] and linked to the anomalous π Berry phase which leads to a zero energy Landau level in magnetic field [7,8].

It was also predicted that orbital magnetism can be paramagnetic rather than diamagnetic. In particular, graphene is expected to exhibit two paramagnetic characteristics: (i) a paramagnetic plateau [4,5,9,10] on either side of the Dirac (DP) or charge neutrality point (CNP) and (ii) logarithmic paramagnetic divergences when the Fermi energy coincides with saddle points (SP) of the graphene band structure [4]; see Fig. 1(a). Such paramagnetic orbital susceptibility peaks proportional to the van Hove (vH) singularities in the density of states (DOS) $\rho(\epsilon)$ were predicted long ago at saddle points of the band structure of any 2D crystalline materials by Vignale [11]. A simple physical explanation of the paramagnetic sign lies in the opposite signs of effective masses m_x and m_y at the saddle points and the fact that the Landau-Peierls susceptibility is proportional to $-\rho(\epsilon)/m_x m_y$. In a magnetic field, near a saddle point, carriers follow hyperboliclike trajectories in reciprocal space. Tunneling between these trajectories gives rise to reconstructed quasicircular paramagnetic trajectories around the saddle points; see Fig. 1(c). Reaching these saddle points in pure graphene requires doping to unattainable Fermi levels of the order of the nearest neighbor hopping energy $t = 2.7$ eV. However, in the following we show how, by inducing a large wavelength moiré periodicity in graphene aligned to a hexagonal boron nitride crystal (h-BN), we can reach such saddle points in the moiré band structure at reasonable doping and detect the expected singular paramagnetic orbital response.

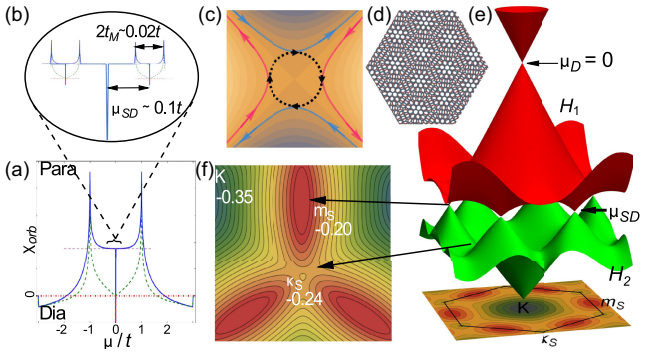

FIG. 1. (a) Orbital susceptibility of graphene. Diamagnetic divergent susceptibility is expected at $\mu = 0$ and paramagnetic divergences at the saddle points at $\mu = \pm t$ (adapted from Ref. [9]). (b) Qualitative expectation of the orbital susceptibility of a graphene/h-BN moiré at low energy as a function of the chemical potential. (c) Explanation of the existence of paramagnetic currents in the reciprocal space close to a saddle point in a 2D crystal (adapted from Ref. [11]). (d) Schematic representation of a moiré lattice obtained with the superposition of two honeycomb lattices of different periods. (e) Miniband structure obtained from the diagonalization of the low energy Hamiltonian of graphene in the presence of a moiré potential of amplitude $t_M = -23$ meV. The two highest energy hole bands are represented below the main graphene Dirac point. They display satellite Dirac points at the m_S points of the mini-Brillouin zone. (f) Isoenergy lines of the lowest hole band (H_2).

Because of the small difference between h-BN and graphene lattice parameters, the moiré lattice parameter a_M of graphene aligned on h-BN is much larger than the size of the unit cell of graphene [see Fig. 1(d)]. The large period moiré potential leads to the formation of low energy minibands centered on each Dirac point [see Fig. 1(e)] and the occurrence of low energy satellite Dirac points (sDP) (at $\mu_{\mathrm{sDP}} \simeq \pm t/10$). These sDPs, accessible by applying moderate gate voltages, were observed experimentally by several groups including Refs. [12–16]. They are surrounded by saddle points whose associated vH singularities were detected via DOS measurements [12]. Saddle points were also revealed in electron focusing experiments [17] and more indirectly in magnetic field dependent patterns in Josephson junctions [18]. Field dependent peaks in photoemission spectra [19] as well as in thermoelectric Hall measurements [20] were interpreted as related to orbital magnetization at low energy vH singularities.

In this Letter we present direct magnetization measurements on graphene/h-BN moiré samples in a wide range of chemical potential. Our experiments reveal the paramagnetic susceptibility singularities predicted long ago at saddle points of the moiré dispersion relation.

Moiré samples and magnetic detection.—In order to reach the satellite Dirac points and the neighboring saddle points at moderate doping, we fabricated samples where the h-BN and graphene lattices were nearly aligned, leading to the maximum value of the graphene/h-BN moiré superlattice parameter as described in Supplemental Material (SM) [21]. We investigated two different samples, M_A and M_B. Raman spectroscopy was used to verify the alignment (see SM and Refs. [16,24]) and determine the lattice parameters yielding $a_{M_A} = 9.5 \pm 0.5$ nm and $a_{M_B} = 12.5 \pm 0.5$ nm corresponding to 1° and 0.6° mismatch angles, respectively (see SM for more details).

The magnetization experiments were performed at 4.2 K using the technique described in Ref. [25]. The encapsulated samples are deposited on a magnetic field detector based on a pair of highly sensitive giant magnetoresistance (GMR) probes [26–28]. The key point of using these sensors is that whereas the orbital magnetism in the system is generated in response to the out-of-plane external field, the GMR probes are only sensitive to the in-plane components of the stray field created by the orbital currents. Connecting the two GMR strips in a Wheatstone bridge configuration and modulating dc gate voltage V_g with an ac bias [Fig. 2(c)] eliminates most of the extraneous spurious magnetic contributions. In this way, one obtains the V_g derivative of the magnetization of the graphene area situated below the gate electrode between the GMR detectors. Additional electrodes outside the GMR detection region allow for transport measurements and an independent determination of the main and satellite Dirac point positions. For an applied out-of-plane magnetic field of

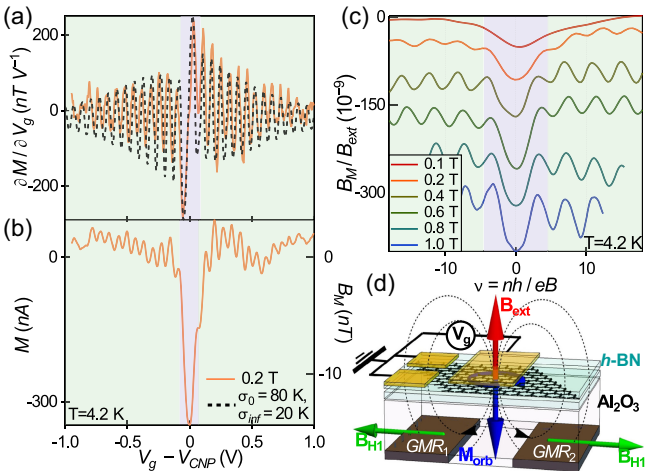

FIG. 2. Low doping data on sample M_A. (a) Solid line: derivative of the magnetic field detected by the GMR detector as a function of the gate voltage V_g close to the DP at $B = 0.2$ T. Dashed line: theoretical gate dependence of $\partial M/\partial V_g$. (b) Magnetization per unit surface obtained by integration of the data in (a) with, on the right-hand axis, units of the equivalent measured magnetic field by the GMR detector. (c) Evolution of the McClure peak and dHvA oscillations for different magnetic fields. On the y axis the detected magnetic signal on the GMR detector is normalized by the applied field. On the x axis $\nu = n\Phi_0/B$ is the Landau level's filling factor where n is the carrier density. (d) Sketch of the experimental setup. $\partial M/\partial V_g$ is measured by the voltage between the two dc current biased GMR detectors R_1 and R_2 at the modulation frequency of the gate voltage.

0.1 T, the in-plane sensitivity of the GMR probes coupled to M_A and M_B are, respectively, 2.5 and 1 Ω/mT and their field equivalent noise is about 1 nT/$\sqrt{\text{Hz}}$.

Main Dirac point region.—As shown in Fig. 2, the magnetization close to Dirac or charge neutrality point (DP) features the diamagnetic McClure peak [25]. This peak broadens with out-of-plane magnetic field, and de Haas–van Alphen (dHvA) oscillations appear with increasing doping. Figure 2 shows both the derivative of the magnetization and the integrated curve as a function of the gate voltage for sample M_A at 0.2 T. The amplitude of the detected signal B_M is 15 nT at the DP. This data can be precisely described deriving the magnetization from the field dependence of the grand potential of graphene at a chemical potential fixed by the gate voltage [25]. The Landau energy levels in graphene are $\epsilon_N = \pm\sqrt{N}\epsilon_B$, with $\epsilon_B = \sqrt{2ev^2\hbar B}$, where v is the Fermi velocity and N is an integer [6]. Disorder is modeled by a Gaussian distribution of chemical potential μ whose standard deviation σ_μ decreases at high doping, due to screening effects which are more efficient. The magnetization was shown to be a universal function of the variables μ/ϵ_B and σ/ϵ_B. The McClure peak at low field has a width $\sigma_0 = 80 \pm 5$ K at the DP. dHvA oscillations observed at larger doping exhibit a characteristic energy scale of $\sigma_\infty = 20$ K. Both σ_0 and σ_∞ are twice smaller than in our previous work [25] and indicate a better quality of the present samples. The dashed curve in Fig. 2(a) is the theoretical fit for $\partial M/\partial V_g$ using those parameters. Figure 2(c) shows the evolution of the magnetization with Landau level filling factor for different field values. The magnetization is renormalized by the applied magnetic field, which in the linear regime is the magnetic susceptibility $\chi = M/B$. One notes the increased dHvA oscillations relative to the McClure response as magnetic field increases.

Satellite Dirac points, paramagnetic singularities.—We now turn to the higher doping regime. Figure 3(a) shows the four-terminal resistance of sample M_A in a wide range of gate voltage. Both satellite peaks are clearly visible at −16 and 15.5 V from the DP. Figure 3(b) shows the magnetization response at 0.2 T in the same range of gate voltage, using a 100 mV modulation of the gate voltage. This strong V_g modulation increases the detection sensitivity at high gate voltage but, because the chemical potential scales as $\sqrt{|V_g|}$, damps the previously discussed diamagnetic McClure response and dHvA oscillations. In the high doping region of interest here, in particular in the region where the sDPs are found in the resistance measurement, we find a series of three antisymmetric peaks, compatible with the expected moiré band orbital magnetism as shown below. The integrated trace displayed in Fig. 3(c) features a diamagnetic peak (red arrow) in the hole doped region at $V_g - V_{\text{DP}} = -17$ V surrounded by two paramagnetic peaks (black arrows). In the electron doped region, we find similar features showing though somehow different positions of the peaks with an asymmetry in the position of the two

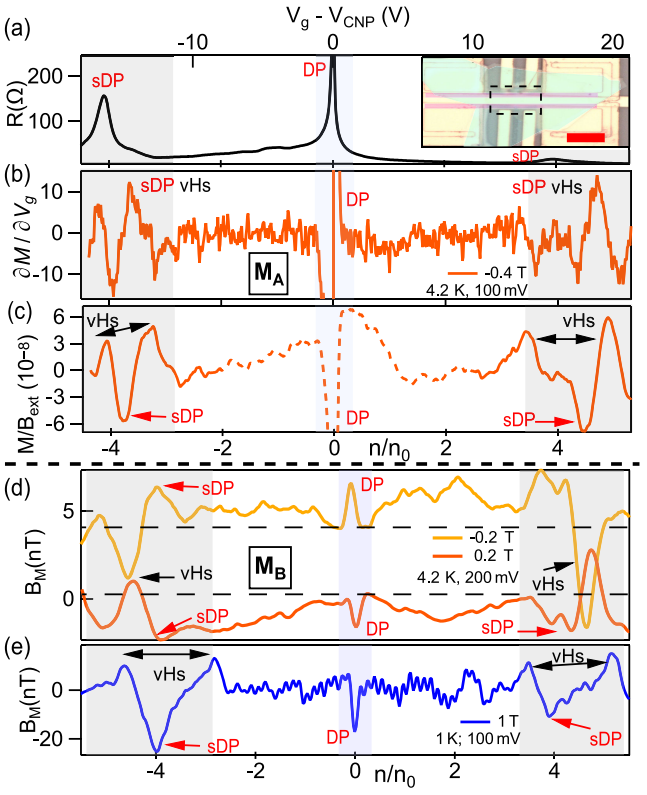

FIG. 3. (a) Four-terminal resistance of sample M_A. Inset: optical image of the sample M_A on the top of the GMR detector (red scale bar is 10 μm). (b) Derivative of the magnetization as a function of the gate voltage and carrier density (renormalized to the moiré filling factor n_0) for a wide doping range in an external magnetic field of 0.2 T for the same sample. (c) Magnetization (in units of the magnetic field detected on the GMR probes, renormalized by the out-of-plane applied field) obtained by integration of the data in (b. In the region of the secondary Dirac peaks we observe diamagnetic peaks (red arrows) surrounded by paramagnetic peaks (black arrows). (d),(e) GMR data measured on sample M_B. at ±0.2 T (D) and 1 T (E).

paramagnetic peaks with respect to the diamagnetic one. From the value of moiré lattice parameter we find that the gate voltage positions of the diamagnetic peaks correspond, as expected, to a carrier density of $4n_0$, where n_0 is the number of carriers per moiré cell (the factor 4 comes from spin and valley degeneracies). The peak positions differ slightly from those observed on the resistance measurements shown in Fig. 3(a), a discrepancy we attribute to the different sample region probed in the resistance measurements [29]. We assign the paramagnetic peaks to the expected magnetic orbital response at the saddle points of the moiré miniband structure. This is the main result of our Letter. Using the gate capacitance of sample M_A, we determine the energy splitting between the paramagnetic and diamagnetic peaks and therefore the expected positions of the vH singularities to be in the range of 10–20 meV. This yields an estimate of the amplitude t_M of the moiré potential [see Fig. 1(b)], as will be discussed more precisely below.

Figures 3(d) and 3(e) present equivalent data on sample M_B. At high hole and electron doping one identifies several peaks of similar amplitude. The diamagnetic satellite peaks occur also at $n_0 = \pm 2$ corresponding to smaller gate voltages ± 12 V than for M_A, consistent with the larger moiré cell area of this sample. There as well, dHvA oscillations are attenuated by the gate voltage modulation of 100 mV and invisible at ± 0.2 T, but are visible at 1 T due to their larger period. The data taken at ± 0.2 T display peaks of opposite sign, approximately at the same positions and with 5 times smaller amplitude than the 1 T data which is consistent with a linear field dependent magnetization. However, in contrast with the M_A data, whereas the diamagnetic satellite Dirac peaks and outer paramagnetic peaks are clearly visible, the inner smaller paramagnetic peaks are nearly undetectable at ± 0.2 T. They are, however, clearly visible at 1 T. In that case, the magnetic energy scale ϵ_B is equal to 30 meV at 1 T; i.e., it is of the order of the moiré potential t_M. The zero-field miniband spectrum discussed below can explain the t_M dependent asymmetry in position and amplitude of paramagnetic singularities but cannot describe this last data at 1 T significantly different from the lower field data ($\epsilon_B \ll t_M$).

Comparison with a simple theoretical model.—The orbital magnetic susceptibility reflects the zero-field moiré miniband structure: at zero temperature and in the absence of disorder, a Dirac point leads to a McClure diamagnetic δ-function divergence [6] and a saddle point to a Vignale paramagnetic logarithmic divergence [11]:

$$\chi_V \simeq \mu_0 \frac{e^2}{24\pi^2} \frac{1}{\sqrt{|m_x m_y|}} \ln \frac{\epsilon_c}{|\mu|}, \tag{1}$$

where $m_{x,y}$ are effective masses and ϵ_c is a cutoff (see SM [21]).

The computation of energy minibands relies on a specific model for the moiré potential [12,30–32]. Here, we use the simplest model (see SM [21]), initially derived in Ref. [12], which considers graphene Dirac electrons moving in the presence of a C_6-symmetric moiré potential of lattice parameter a_M and amplitude t_M. We do not consider inversion symmetry breaking [19,31]. The minibands can easily be calculated as shown in Figs. 1 and 4 and the SM. The main features are satellite Dirac cones and saddle points. There is a clear electron-hole asymmetry determined by the amplitude and sign of t_M. This is illustrated in Fig. 4 showing cuts along the K, κ_S, m_S, K directions of the three lowest electron (E_1, E_2, and E_3) and highest hole (H_1, H_2, and H_3) minibands around the main DP. The sDPs (red arrows in Fig. 4) occur between E_1 and E_2 at m_S and κ_S, between H_1 and H_2 at m_S, and between H_2 and H_3 at κ_S. Saddle points (indicated as vHs by arrows in Fig. 4) occur in E_1 and H_1 close to m_s along $[m_S, \kappa_S]$, in E_2 close to κ_S along $[\kappa_S, m_S]$, and in H_2 close to κ_S along $[\kappa_S, K]$.

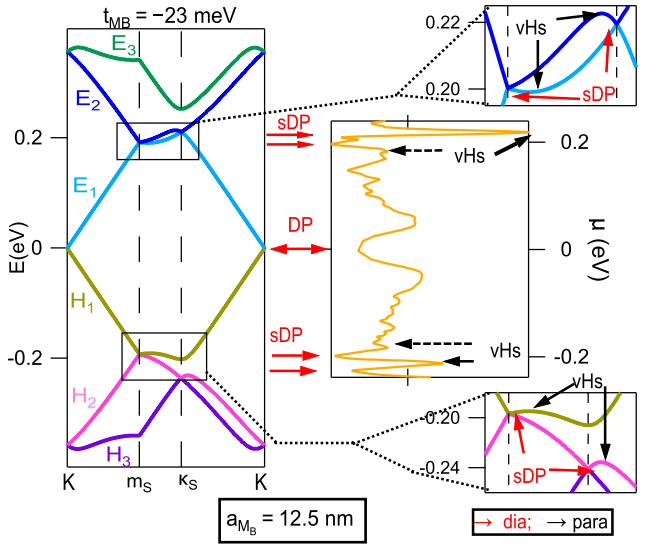

FIG. 4. Comparison between band structure (left) and experimental data at 0.2 T and 4.2 K for sample M_B (right). We present cuts along the three K, m_S, m_S, κ_S, and κ_S, K axes of the moiré band structure calculated for $t_M = -23$ meV matching the position of the observed diamagnetic peaks (red arrows) and paramagnetic peaks (black plain and dotted arrows) in magnetization data function of the chemical potential. Dotted black arrows point toward barely visible paramagnetic peaks at saddle points because they are very close in energy to the satellite m_S Dirac points, as shown more precisely in SM [21].

We determine t_M by comparing the chemical potential position of the measured satellite diamagnetic and paramagnetic peaks (at low magnetic field) with their expected energy positions according to the band structure calculation (at zero magnetic field). The best agreement is obtained for $t_M = -15$ meV (sample M_A) and $t_M = -23$ meV (sample M_B) as shown in SM [21] and Fig. 4 for sample M_B. On the electron side, the sDPs at m_S and κ_S are at slightly different energies, which is compatible with the split diamagnetic peak shown in Fig. 4. On the hole side, the measured splitting is larger, also consistent with the calculated sDPs at m_S and κ_S that are more separated in energy. As seen in Fig. 4, the sequence of paramagnetic and diamagnetic peaks is different on the electron and hole sides. This sequence can be reproduced by choosing $t_M < 0$.

The shape and curvature of the minibands (see Fig. 4 and SM [21]) in the vicinity of the κ_S and m_S points help explain the asymmetry in position and amplitude of the paramagnetic peaks. These are clearly more pronounced on the high doping sides of sDPs. We find that the curvatures are much larger in E_2 and H_2 compared to E_1 and H_1. As a result the position in energy of the saddle points on the low doping minibands (E_1 and H_1) are very close to the m_S sDP, in contrast with their position at large doping (E_2 and H_2) located further in energy above κ_S. We show in SM (Secs. I.C and I.E) that these observations explain why the outer paramagnetic peaks are more intense than the inner

peaks (tending to overlap with the diamagnetic peaks at the m_S sDPs), both on electron and hole sides. This asymmetry is more pronounced for sample M_B whose moiré amplitude $|t_M|$ is stronger than for M_A.

In order to compare the amplitudes of the measured magnetization singularities to theoretical predictions, we first estimate the ratio between the diamagnetic peaks at the satellite and main Dirac points. The orbital susceptibility χ_M of graphene at the main Dirac point depends on the square of the Fermi velocity v and the disorder standard deviation σ_0 according to $\chi_M \propto -v^2/\sigma_0$ [6,25]. We assume that such a relation remains true for the susceptibility $\chi_S \propto -v_S^2/\sigma_S$ at an m_S sDP with $v_S \simeq 0.35v$ and $\sigma_S \simeq 0.65\sigma_0$ (see SM [21]). Taking into account that there are 3 times more m_S than K points, this leads to the ratio $r = 3(\chi_S/\chi_M) = 3(v_S^2\sigma_0/v^2\sigma_S) \simeq 0.55 \pm 0.1$ for sample M_B to be compared to the measured $r = 0.33 \pm 0.1$.

Turning to the paramagnetic susceptibility peaks, we show in SM [21] how one can also estimate their amplitude from Eq. (1) and the calculated effective masses of the saddle points. The average curvature $|m_x m_y|^{-1/2}$ is of the order of $200m_e^{-1}$ for all investigated bands, where m_e is the free electron mass, explaining the large amplitude of the paramagnetic peaks.

Experiments show that the paramagnetic peaks above the sDPs in the electron doped region are of the same order of magnitude as the diamagnetic peaks at the sDPs. This surprising feature can be explained by taking disorder into account. Despite the logarithmic (paramagnetic) divergence being weaker than the δ function (diamagnetic) divergence, the disorder rounding is stronger for the diamagnetic than for the paramagnetic peak, rendering the two peaks of similar magnitude (see SM [21]).

In conclusion, our measurements of the orbital magnetization of graphene with a moiré potential show a rich set of singularities of the orbital magnetization in the vicinity of sDPs. These consist of diamagnetic peaks at the satellite Dirac points surrounded by paramagnetic peaks which can be associated to the van Hove singularities of the DOS at the saddle points of the miniband structure induced by the moiré potential. These experiments therefore confirm the long-standing theoretical predictions of the existence of paramagnetic orbital magnetism in 2D materials at van Hove singularities which, in the case of the graphene/h-BN moiré investigated here, exceeds by far the Pauli susceptibility (see SM [21]). A natural prolongation of this Letter would be to measure the orbital magnetization of graphene bilayer moiré structures also extensively investigated [33–36] with the possibility to obtain ferromagnetic orbital phases [35]. It is also interesting that the typical amplitude of the paramagnetic susceptibility peaks we measure is of the same order of magnitude as the values predicted for graphene bilayer moirés close to the magic angle [36]. This singular paramagnetic orbital magnetism is shown to possibly lead to the emergence of new kinds of correlated phases when the sample is embedded in a quantum electromagnetic cavity. Our results also motivate the extension of this Letter to twisted graphene bilayers with larger moiré periods in which field periodic orbital currents are expected [37].

The authors thank E. Paul of SPEC-CEA for the GMR sensors' patterning and R. Weil and S. Autier-Laurent of LPS for Nanofabrication and Cryogenic support. They also acknowledge fruitful discussions with A. Chepelianskii, F. Parmentier, R. Delagrange, D. Mailly, C. Mora, and P. Simon and financial support from the BALLISTOP ERC 66566 advanced grant. This work benefited from the C2N micro nanotechnologies platforms and is partially supported by the RENATECH network, the General Council of Essonne, and the DIM-SIRTEC. R. R.-P. acknowledges the ERC starting grant TWISTRONICS. K. W. and T. T. acknowledge support from JSPS KAKENHI (Grants No. 19H05790, No. 20H00354, and No. 21H05233).

[1] L. Landau, Z. Phys. **64**, 629 (1930).
[2] R. Peierls, Z. Phys. **80**, 763 (1933).
[3] D. Xiao, M. C. Chang, and Q. Niu, Rev. Mod. Phys. **82**, 1959 (2010).
[4] A. Raoux, M. Morigi, J. N. Fuchs, F. Piéchon, and G. Montambaux, Phys. Rev. Lett. **112**, 026402 (2014).
[5] Frédéric Piéchon, Arnaud Raoux, J. N. Fuchs, and Gilles Montambaux, Phys. Rev. B **94**, 134423 (2016).
[6] J. W. McClure, Phys. Rev. **104**, 666 (1956).
[7] G. P. Mikitik and Yu. V. Sharlai, Phys. Rev. Lett. **82**, 2147 (1999).
[8] J. N. Fuchs, F. Piéchon, M. O. Goerbig, and G. Montambaux, Eur. Phys. J. B **77**, 351 (2010).
[9] A. Raoux, F. Piéchon, J. N. Fuchs, and G. Montambaux, Phys. Rev. B **91**, 085120 (2015).
[10] G. Gómez-Santos and T. Stauber, Phys. Rev. Lett. **106**, 045504 (2011).
[11] G. Vignale, Phys. Rev. Lett. **67**, 358 (1991).
[12] M. Yankowitz, J. Xue, D. Cormode, J. D. Sanchez-Yamagishi, K. Watanabe, T. Taniguchi, P. Jarillo-Herrero, P. Jacquod, and B. J. LeRoy, Nat. Phys. **8**, 382 (2012).
[13] B. Hunt, J. D. Sanchez-Yamagishi, A. F. Young, M. Yankowitz, B. J. LeRoy, K. Watanabe, T. Taniguchi, P. Moon, M. Koshino, P. Jarillo-Herrero, and R. C. Ashoori, Science **340**, 1428 (2013).
[14] C. R. Dean, L. Wang, P. Maher, C. Forsythe, F. Ghahari, Y. Gao, J. Katoch, M. Ishigami, P. Moon, M. Koshino, T. Taniguchi, K. Watanabe, K. L. Shepard, J. Hone, and P. Kim, Nature (London) **497**, 598 (2013).
[15] C. R. Woods, L. Britnell, A. Eckmann, R. S. Ma, J. C. Lu, H. M. Guo, X. Lin, G. L. Yu, Y. Cao, R. V. Gorbachev, A. V. Kretinin, J. Park, L. A. Ponomarenko, M. I. Katsnelson, Yu. N. Gornostyrev, K. Watanabe, T. Taniguchi, C. Casiraghi, H. J. Gao, A. K. Geim, and K. S. Novoselov, Nat. Phys. **10**, 451 (2014).
[16] R. Ribeiro-Palau, C. Zhang, K. Watanabe, T. Taniguchi, J. Hone, and C. R. Dean, Science **361**, 690 (2018).

[17] Menyoung Lee, John R. Wallbank, Patrick Gallagher, Kenji Watanabe, Takashi Taniguchi, Vladimir I. Fal'ko, and David Goldhaber-Gordon, Science **353**, 1526 (2016).
[18] D. I. Indolese, R. Delagrange, Péter Makk, J. R. Wallbank, K. Wanatabe, T. Taniguchi, and Christian Schonenberger, Phys. Rev. Lett. **121**, 137701 (2018).
[19] Sanfeng Wu, Lei Wang, You Lai, Wen-Yu Shan, Grant Aivazian1, Xian Zhang, Takashi Taniguchi, Kenji Watanabe, Di Xiao, Cory Dean, James Hone, Zhiqiang Li, and Xiaodong Xu, Sci. Adv. **2**, e1600002 (2016).
[20] R. Moriya, K. Kinoshita, J. A. Crosse, K. Watanabe, T. Taniguchi, S. Masubuchi, P. Moon, M. Koshino, and T. Machida, Nat. Commun. **11**, 1 (2020).
[21] See Supplemental Material at http://link.aps.org/supplemental/10.1103/PhysRevLett.131.116201 for the theoretical calculations from the miniband structure of graphene with a moiré potential and extra experimental data, which includes Refs. [22–24].
[22] N. F. Q. Yuan and L. Fu, Phys. Rev. B **101**, 125120 (2020).
[23] F. Pizzocchero, L. Gammelgaard, B. S. Jessen, J. M. Caridad, L. Wang, J. Hone, P. Böggild, and T. J. Booth, Nat. Commun. **7**, 11894 (2016).
[24] A. Eckmann, J. Park, H. Yang, D. Elias, A. S. Mayorov, G. Yu, R. Jalil, K. S. Novoselov, R. V. Gorbachev, M. Lazzeri, A. K. Geim, and C. Casiraghi, Nano Lett. **13**, 5242 (2013).
[25] J. Vallejo Bustamante, N. J. Wu, C. Fermon, M. Pannetier-Lecoeur, T. Wakamura, K. Watanabe, T. Tanigushi, T. Pellegrin, A. Bernard, S. Daddinounou, V. Bouchiat, S. Guéron, M. Ferrier, G. Montambaux, and H. Bouchiat, Science **374**, 1399 (2021).
[26] M. N. Baibich, J. M. Broto, A. Fert, F. Nguyen Van Dau, F. Petroff, P. Etienne, G. Creuzet, A. Friederich, and J. Chazelas, Phys. Rev. Lett. **61**, 2472 (1988).
[27] B. Dieny, V. S. Speriosu, S. S. P. Parkin, B. A. Gurney, D. R. Wilhoit, and D. Mauri, Phys. Rev. B **43**, 1297 (1991).
[28] P. A. Guitard, R. Ayde, G. Jasmin-Lebras, L. Caruso, M. Pannetier-Lecoeur, and C. Fermon, Appl. Phys. Lett. **108**, 212405 (2016).
[29] For samples M_A the position in gate voltage of the diamagnetic peaks differs by 2 V compared to the resistance peaks. This offset which corresponds to a 5% shift in chemical potential can be attributed to the small size of the gate compared to the size of the sample measured in transport.
[30] P. Moon and M. Koshino, Phys. Rev. B **90**, 155406 (2014).
[31] J. R. Wallbank, A. A. Patel, M. Mucha-Kruczyński, A. K. Geim, and V. I. Fal'Ko, Phys. Rev. B **87**, 245408 (2013).
[32] J. Jung, A. M. DaSilva, A. H. MacDonald, and S. Adam, Nat. Commun. **6**, 1 (2015).
[33] Guohong Li, A. Luican, J. M. B. Lopes dos Santos, A. H. Castro Neto, A. Reina, J. Kong, and E. Y. Andrei, Nat. Phys. **6**, 109 (2010).
[34] Eva Y. Andrei, Dmitri K. Efetov, Pablo Jarillo- Herrero, Allan H. MacDonald, Kin Fai Mak, T. Senthil, Emanuel Tutuc, Ali Yazdani, and Andrea F. Young, Nat. Mater. Rev. **6**, 201 (2021).
[35] Sameer Grover, Matan Bocarsly, Aviram Uri, Petr Stepanov, Giorgio Di Battista, Indranil Roy, Jiewen Xiao, Alexander Y. Meltzer, Yuri Myasoedov, Keshav Pareek, Kenji Watanabe, Takashi Taniguchi, Binghai Yan, Ady Stern, Erez Berg, Dmitri K. Efetov, and Eli Zeldov, Nat. Phys. **18**, 885 (2022).
[36] D. Guerci, P. Simon, and C. Mora, Phys. Rev. B **103**, 224436 (2021); Gian Marcello Andolina *et al.*, arXiv:2210.10371.
[37] S. G. Xu, A. I. Berdyugin, P. Kumaravadivel, F. Guinea, R. Krishna Kumar, D. A. Bandurin, S. V. Morozov, W. Kuang, B. Tsim, S. Liu, J. H. Edgar, I. V. Grigorieva, V. I. Fal'ko, M. Kim, and A. K. Geim, Nat. Commun. **10**, 4008 (2019).